Influence of Edge Defects, Vacancies, and Potential Fluctuations on Transport Properties of Extremely Scaled Graphene Nanoribbons

Mirko Poljak, *Student Member, IEEE*, Emil B. Song, Minsheng Wang, Tomislav Suligoj, *Member, IEEE*, and Kang L. Wang, *Fellow, IEEE*

***Abstract*—Atomistic quantum transport simulations of a large ensemble of devices are employed to investigate the impact of different sources of disorder on the transport properties of extremely scaled (length of 10 nm and width of 1–4 nm) graphene nanoribbons. We report the dependence of the transport gap, ON- and OFF-state conductances, and ON–OFF ratio on edge-defect density, vacancy density, and potential fluctuation amplitude. For the smallest devices and realistic lattice defect densities, the transport gap increases by up to $\sim$300%, and the ON–OFF ratio reaches almost $\sim 10^6$. We also report a rather high variation of the transport gap and ON–OFF ratio. In contrast, we find that the potential fluctuations have a negligible impact on the transport gap and cause a relatively modest increase of the ON–OFF ratio.**

***Index Terms*—Edge defects, graphene nanoribbons (GNRs), nonequilibrium Green's function (NEGF) simulation, potential fluctuations, transport gap, vacancies.**

I. Introduction

NOVEL device architectures and alternative materials have been investigated in order to solve the issues of transistor scaling in complementary metal–oxide–semiconductor (CMOS) technology [1], [2]. Among many candidates, graphene-based nanoelectronic devices have attracted a tremendous research interest due to high carrier mobility and compatibility with the conventional planar technology [3]. The problem of metallicity of large-area graphene, which causes high OFF-state leakage and low ON–OFF current ratios, is solved by employing graphene nanoribbons (GNRs) that exhibit bandgaps because of geometric quantum confinement [4]–[6]. Due to the hyperbolic dependence of the bandgap on GNR width [7]–[10], acceptable widths are determined by the acceptable bandgaps necessary for specific CMOS applications. According to [2], GNR-based field-effect transistors (FETs) could replace silicon FETs at the 12-nm technology node, which corresponds to the channel length of approximately 10 nm. Therefore, the investigation of ultrashort ($L \sim 10$ nm) and ultranarrow ($W < 5$ nm) GNRs is necessitated by scaling and demands on acceptable bandgaps.

In order to properly assess GNR performance and the applicability of extremely scaled GNRs in CMOS, realistic GNRs must be investigated. The study should account for the effects of different disorders that arise from the nonidealities of the fabrication process and impurities in the substrate. The influence of disorder in graphene has been studied recently [11]–[13]. However, the reports on the effects of disorder in GNRs are limited mostly to the influence of edge defects and for very large GNRs [10], [14], relatively small ensembles of simulated devices [15]–[17], or specific cases of lattice defects [18], [19]. Therefore, a thorough investigation of the influence of all relevant sources of disorder on the transport properties of extremely scaled GNRs is indispensable.

In this paper, we present statistically averaged transport properties obtained from atomistic quantum transport simulations of large ensembles of randomly generated GNR devices. The statistical approach is mandatory due to the high variability of GNR properties caused by disorder, which is even more prominent in extremely scaled GNRs that are of interest for the end-of-the-roadmap CMOS. We report the behavior of the transport gap, ON- and OFF-state conductances, and ON–OFF ratio at 300 K for various disorder strengths for edge defects, vacancies, and potential fluctuations.

II. Numerical Modeling

Atomistic simulations based on a tight binding (TB) Hamiltonian with a single p_z orbital basis per carbon atom are employed in this work. For each GNR, we construct the Hamiltonian that accounts for up to the third nearest neighbor interactions, which is given by

$$H = \sum_i \varepsilon_i c_i^\dagger c_i + \sum_{k=1}^{3} t_k \sum_{i,j} c_i^\dagger c_j + \text{H.c.} \qquad (1)$$

Manuscript received June 12, 2012; revised August 29, 2012; accepted September 4, 2012. Date of publication October 9, 2012; date of current version November 16, 2012. M. Poljak acknowledges the support of the U.S. Department of State through the Fulbright Fellowship. M. Poljak and T. Suligoj acknowledge partial financial support from the Ministry of Science, Education and Sports of the Republic of Croatia under Contract 036-0361566-1567. E. B. Song, M. Wang, and K. L. Wang acknowledge financial support from the MARCO Focus Center on Functional Engineered Nano Architectonics. The review of this paper was arranged by Editor A.-C. Seabaugh.

M. Poljak was with the Department of Electrical Engineering, University of California at Los Angeles, Los Angeles, CA 90095, USA. He is now with the Department of Electronics, Microelectronics, Computer and Intelligent Systems, Faculty of Electrical Engineering and Computing, University of Zagreb, 10000 Zagreb, Croatia (e-mail: mpoljak@zemris.fer.hr).

E. B. Song, M. Wang and K. L. Wang are with the Department of Electrical Engineering, University of California at Los Angeles, Los Angeles, CA 90095, USA (e-mail: emil@ee.ucla.edu; minswang@ee.ucla.edu; wang@ee.ucla.edu).

T. Suligoj is with the Department of Electronics, Microelectronics, Computer and Intelligent Systems, Faculty of Electrical Engineering and Computing, University of Zagreb, 10000 Zagreb, Croatia (e-mail: tom@zemris.fer.hr).

Color versions of one or more of the figures in this paper are available online at http://ieeexplore.ieee.org.

Digital Object Identifier 10.1109/TED.2012.2217969

0018-9383/$31.00 © 2012 IEEE

where ε_i is the on-site energy and $c_i^\dagger(c_i)$ is the creation (annihilation) operator while t_1, t_2, and t_3 are the hopping parameters for the nearest, second nearest, and third nearest neighbor interactions taken from [20]. Edge bond relaxation, which is found to increase the bandgap of GNRs [21], is accounted for by using a modified hopping parameter $t_1' = 1.12t_1$ for the edge carbon–carbon bonds [22].

The GNR band structure, density of states (DOS), local DOS (LDOS), and transmission function are calculated by means of the nonequilibrium Green's function (NEGF) formalism [23]. The device Green's function is obtained as

$$G_d = \left[(E + i0^+)I - H - \Sigma_1 - \Sigma_2\right]^{-1} \quad (2)$$

where H is the device Hamiltonian and $\Sigma_{1,2}$ designates the contact self-energy that accounts for the coupling of the device to the contacts. DOS and LDOS are obtained from the spectral function $A(E) = i(G_d - G_d^\dagger)$. The transmission is calculated as $T(E) = \text{Trace}(\Gamma_1 G_d \Gamma_2 G_d^\dagger)$, where the contact broadening function is obtained from $\Gamma_{1,2} = i(\Sigma_{1,2} - \Sigma_{1,2}^\dagger)$. An iterative procedure is used to calculate the surface Green's functions that are needed to obtain the contact self-energies [24], [25].

Edge defects and vacancies are realized by the random removal of single atoms from the edges or the bulk of GNR in the given percentage, P_{ED} for edge defects and P_V for vacancies. Removing single atoms instead of dimers allows a more realistic investigation of the effects of lattice defects because of the bipartite nature of the graphene lattice [12]. In the total Hamiltonian, hopping parameters of the removed atoms are set to zero, i.e., the corresponding orbitals are removed from the TB Hamiltonian. Potential fluctuations are assumed to originate from the charged impurities in the substrate and are implemented in the TB model as a local change in the on-site energy. Fluctuations are randomly generated as positive and negative Gaussian potential profiles [26] with an amplitude δV and a density of approximately 10^{13} cm^{-2}. The density is rather high due to the small area of the nanoribbon, which is on the order of $\sim$10 nm^2. Realistic δV ranges from 50 to 150 mV [27], [28]. The correlation length of the Gaussian profile is set to $\Lambda = 5a_{C-C}$, where a_{C-C} is the carbon–carbon bond length, which is appropriate for remote charged impurities since Λ is sufficiently larger than a_{C-C} [29]. Local charge induced by lattice defects or potential fluctuations is neglected due to a small change of the potential caused by the charge [27], [28], which, in turn, has a negligible influence on the transmission, as reported in Section III. Fig. 1(a) and (b) shows an illustration of a 1.10-nm-wide GNR with lattice defects and an example of normalized potential fluctuations, respectively.

We investigate semiconducting armchair GNRs with the widths in the 1–4-nm range of the same length ($L = 10.1$ nm), and all GNRs belong to the same $3m + 1$ group for consistency. We focus on extremely scaled GNRs (W of 1.10 and 1.84 nm) and compare their properties with those of the wider nanoribbons. GNRs with the width of 1–2 nm and bandgaps of $\sim$0.4 eV have been reported experimentally [9], which deepens further our interest in devices at this scale. For each device and disorder case, we perform an averaging over an ensemble of 100 randomly generated GNRs, which results in over 3400 devices simulated in this work.

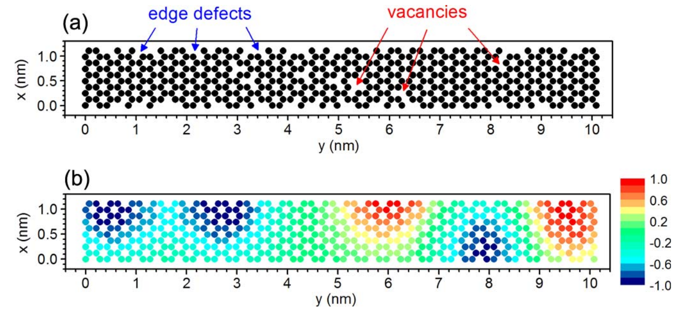

Fig. 1. (a) Random realization of a GNR with edge defects and vacancies. (b) Example of (normalized) randomly generated Gaussian potential fluctuations. $W = 1.10$ nm, and $L = 10.1$ nm.

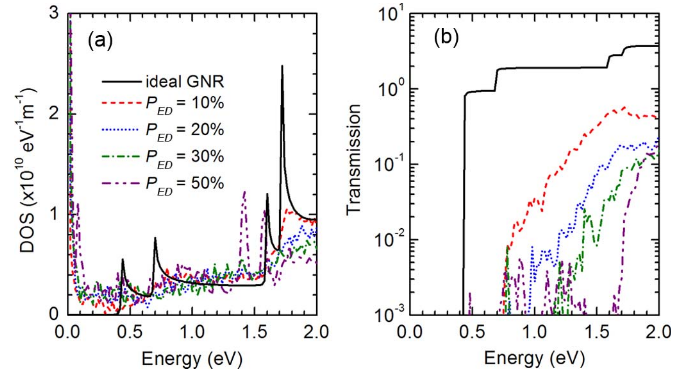

Fig. 2. Influence of edge defects on (a) averaged DOS and (b) averaged transmission, for different edge-defect densities (P_{ED}). GNR width is 1.10 nm.

III. Results and Discussion

The influence of edge defects on DOS and transmission is shown in Fig. 2. The comparison between the DOS of an ideal GNR and averaged DOS curves for different P_{ED}, presented in Fig. 2(a), shows that defected GNRs exhibit nonzero DOS in the bandgap with a peak at $E = 0$ eV. This effect is caused by an uncompensated number of orbitals in two graphene sublattices caused by the random removal of single atoms [12]. Previous reports demonstrate that the states in the gap are strongly localized and do not contribute to conduction according to the mobility-edge theory [10], [14], [30]. Hence, the bandgap does not vanish, which demands the evaluation of the effective transport gap (E_{TG}). Fig. 2(b) shows a comparison between the transmission of the ideal GNR and the averaged transmission curves of edge-defected GNRs. Transmission is suppressed over the whole energy range, and the decrease is stronger for higher P_{ED}. In contrast to the results in [17], the transmission decreases significantly even for low P_{ED}. This difference could be a consequence of removing single atoms on the edges in our approach, which results in more atomic sites with localized states. The most notable effect of introducing edge defects is a significant increase of E_{TG}. For example, the half gap equals $\sim$0.8 eV and $\sim$1.7 eV for P_{ED} of 10% and 50%, respectively. Furthermore, for high edge-defect densities, e.g., $P_{\mathrm{ED}} = 50\%$, the transmission exhibits peaks that reach $\sim$0.01 inside the transport gap, most likely due to quantum hopping between localized states [31]. Due to the high transmission variation

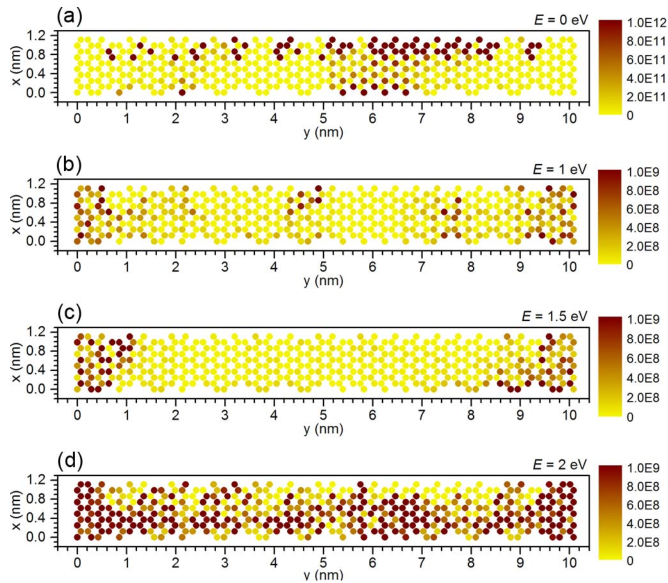

Fig. 3. LDOS of an edge-defected GNR with $P_{\mathrm{ED}} = 50\%$ at different energies of (a) 0 eV, (b) 1 eV, (c) 1.5 eV, and (d) 2 eV. Each atomic site is represented by a circle, and the LDOS magnitude is indicated by color. The legend is in the units of $\mathrm{eV}^{-1}\mathrm{m}^{-1}$. $W = 1.10$ nm.

inside the gap, the ON-state conductance (G_{ON}) will depend strongly on the Fermi energy (E_F) at which G_{ON} is defined. The Fermi level of the GNR can be adjusted by the gate voltage that is set to supply the voltage (V_{DD}) in the ON state in CMOS applications. Therefore, a higher P_{ED} demands an increased V_{DD} to achieve the same G_{ON} as in the case of low P_{ED}. For example, E_F should be set to at least 1 or 1.8 eV if P_{ED} is 10% or 50%, respectively, to obtain comparable conductance in the ON state. However, this is undesirable due to the low supply voltage $(V_{\mathrm{DD}} \leq 0.7$ V) that is projected beyond the 12-nm CMOS technology node [2].

The atomistic NEGF approach used in this work allows the examination of LDOS at any energy. This enables us to find a limit between the localized and extended states and to determine the transport gap, i.e., the mobility edge [10]. Fig. 3 shows the LDOS of the edge-defected GNR with $P_{\mathrm{ED}} = 50\%$ at four different energies in the range from 0 to 2 eV. Localized states are observed even at 1.5 eV [see Fig. 3(c)], whereas an extended state is evident in Fig. 3(d) at $E = 2$ eV, which clearly indicates that the half gap is between 1.5 and 2 eV. This conclusion is in accordance with the transmission curve in Fig. 2(b) that gives a transport gap of ~1.7 eV. We also observe a large number of localized states with a high LDOS at $E = 0$ eV in Fig. 3(a), which explains the high DOS at zero energy in Fig. 2(a). Evidently, finding the transport gap by examining LDOS is a time-consuming procedure since it demands the comparison of a large number of LDOS plots, which calls for a simpler method to separate the localized and extended states.

The DOS and transmission of extremely scaled GNRs are heavily influenced by vacancies, as shown in Fig. 4. Averaged DOS curves for various P_V values, shown in Fig. 4(a), exhibit nonzero DOS in the energy gap with a peak strongly confined at $E = 0$ eV. In the remaining range, the averaged DOS of GNRs with vacancies closely follows the DOS of the ideal GNR, and the smoothing of the Van Hove singularities diminishes as P_V decreases. The comparison of transmission curves presented in Fig. 4(b) shows an increasing E_{TG} with increasing P_V. The transport gap increase is considerably weaker than in the case of edge-defected GNRs since it reaches ~1.1 eV for a very high P_V of 10%. Fig. 4(b) also shows that the transmission is suppressed rather uniformly over the whole energy range, in contrast to edge-defected GNRs where the decrease is stronger at lower energies. Due to the lower transmission variation inside the gap, G_{ON} in GNRs with vacancies should depend less on V_{DD} than in the case of edge defects. Nevertheless, if we compare transmission values at $E = 0.7$ eV (projected supply voltage for the 12-nm CMOS [2]), the transmission decreases approximately 8×, 110×, 229×, and 957× as P_V increases from 1%, over 3% and 5%, to 10%.

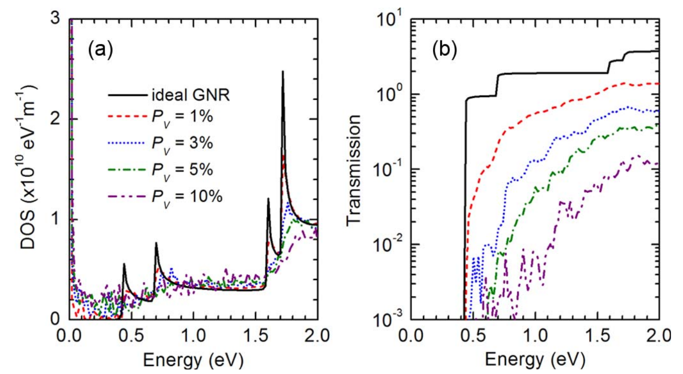

Fig. 4. (a) Averaged DOS and (b) averaged transmission as a function of energy for different vacancy densities (P_V). GNR width is 1.10 nm.

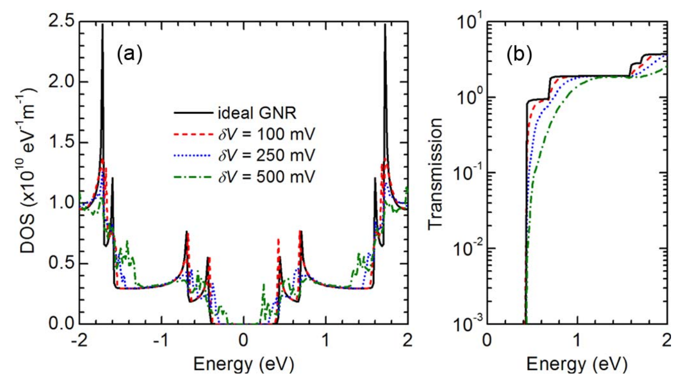

Fig. 5. Dependence of (a) averaged DOS and (b) averaged transmission on energy and the amplitude of potential fluctuations (δV). $W = 1.10$ nm.

Fig. 5 shows the effects of potential fluctuations. Results shown in Fig. 5(a) demonstrate that amplitudes $\delta V \leq 100$ mV have a negligible influence since the bandgap and Van Hove singularities are preserved. In contrast to lattice defects, we find that the potential disorder examined in this work does not induce localized states and high DOS at zero energy. However, some states with nonzero DOS exist in the bandgap for δV of 250 or 500 mV, and we attribute this localization to potential wells formed by fluctuations. We note that DOS is asymmetrical with respect to $E = 0$ eV, i.e., for the electron and hole

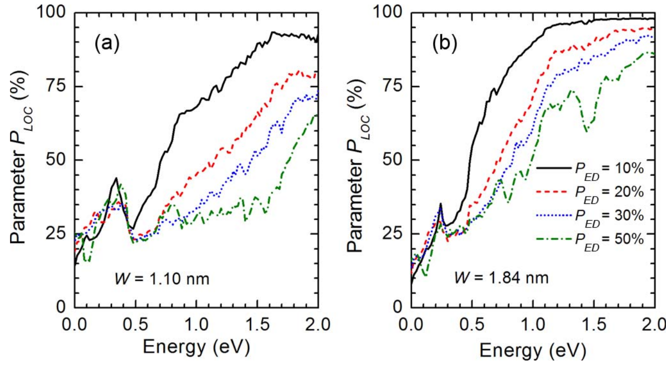

Fig. 6. Dependence of the parameter P_{LOC} defined in the text on energy for GNRs that are (a) 1.10 nm and (b) 1.84 nm wide. Plots show P_{LOC} behavior for four densities of edge defects (P_{ED}).

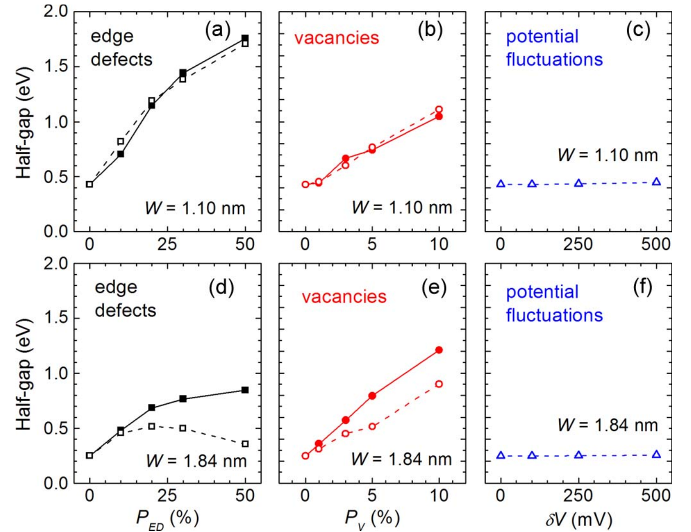

Fig. 7. Dependence of $E_{\mathrm{TG}}/2$ on disorder strength is shown in (a)–(c) for $W = 1.10$ nm and in (d)–(f) for $W = 1.84$ nm. Full symbols and full line denote the P_{LOC}-based half gap, while empty symbols and dashed line are used for the transmission-based half gap.

energy range, due to the randomness of the local shifts in the on-site energy. The comparison of transmission curves shown in Fig. 5(b) demonstrates a relatively weak impact of potential fluctuations, even for the unrealistically high δV of 500 mV. In comparison to edge defects and vacancies, E_{TG} increases only slightly, and the influence of potential disorder on G_{ON} is expected to be modest since the transmission decrease at $E = 0.7$ eV equals 1.5×, 2.0×, and 3.9× as δV increases from 100 mV, over 250 mV, to 500 mV. Potential fluctuations cause elastic scattering, in contrast to lattice defects that cause inelastic scattering which is far more effective in reducing the transmission. The transport regime in the ON state can be examined by calculating the mean free path (λ), as was done for edge-defected GNRs in [25]. As δV increases from 100 to 500 mV, λ decreases from 13.2 to 2.9 nm, which indicates ballistic transport for $\delta V \leq 100$ mV, i.e., for realistic amplitudes. The weak influence of potential fluctuations justifies our decision to neglect the induced local charges and the corresponding potential change, which discards the need to solve the Poisson equation. For other disorder cases, the transport is diffusive because we obtain $\lambda < 1.3$ nm $\ll L$.

In addition to the E_{TG} values extracted from the transmission, we also find E_{TG} using an energy-dependent parameter that enables the separation of extended and localized states. For each energy, we count the number of atomic sites (N_η) that exhibit an LDOS value higher than $\eta = 5\%$ of the maximum LDOS at that energy. The parameter is then calculated as

$$P_{\mathrm{LOC}} = 100\% \cdot N_\eta/(N_{\mathrm{TOT}} - N_R) \quad (3)$$

where N_{TOT} is the total number of atoms and N_R is the number of removed atoms. This parameter should be smaller in the range of localized states than for extended states because N_η is small for localized states. Hence, P_{LOC} can be interpreted as an indicator of localization strength. For the ideal GNR, P_{LOC} is $\sim$100%. The parameter is shown in Fig. 6 for the case of edge defects for GNR widths of 1.10 nm [see Fig. 6(a)] and 1.84 nm [see Fig. 6(b)]. As P_{ED} increases, P_{LOC} decreases over the whole energy range for both devices due to the increased generation of localized states. Going from $E = 2$ eV down to 0 eV, P_{LOC} is almost constant to a certain limit (particularly for the wider GNR) and then decreases abruptly as energy decreases, which indicates extended states at high energies and enhanced localization effects at low energies. This behavior allows us to define a transport gap within the mobility-edge approach [30] via P_{LOC} curves. We extract the P_{LOC}-based E_{TG} as the energy range where P_{LOC} is less than 50% and compare it to the transmission-based E_{TG} that is extracted as the energy range in which the transmission is lower than 0.01.

The dependence of the half gap on the strength of different disorders is shown in Fig. 7 for the two examined GNRs. Due to weak localization, P_{LOC} does not reach 50% in the case of potential fluctuations, and it is therefore possible only to extract the transmission-based E_{TG}, as shown in Fig. 7(c) and (f). For $W = 1.10$ nm, E_{TG} curves exhibit an almost identical behavior in Fig. 7(a) and (b). However, a strong discrepancy between the two methods can be seen in the case of $W = 1.84$ nm for which the half-gap curves diverge as P_{ED} or P_V increases [see Fig. 7(d) and (e)]. This disagreement is consistently observed in GNRs with $W > 1.84$ nm (not shown here), and it renders the mobility-edge approach inadequate for the extraction of the transport gap in extremely scaled GNRs. Nevertheless, P_{LOC}-based E_{TG} offers a valuable physical insight; namely, there exists a range of localized states that conduct well since the transmission-based E_{TG} is smaller than the P_{LOC}-based E_{TG}. In other words, the transmission can exhibit peaks at certain energies even though the states are localized, as indicated by the parameter P_{LOC}, which indicates that quantum hopping between localized states most likely enhances the transmission [32], [33] and decreases the transmission-based E_{TG}. This effect could be responsible for the unexpectedly low bandgap (< 0.5 eV) observed in sub-5-nm-wide GNRs reported in [9].

Edge defects have the greatest influence on the transport gap, as shown in Fig. 7(a) and (d). For $P_{\mathrm{ED}} = 50\%$, the transmission-based half gap increases by 299% and 43% for W of 1.10 and 1.84 nm, respectively. In comparison, the P_{LOC}-based method predicts enhancements of 311% and 241%,

which also predict a higher immunity of wider GNRs. In contrast, the half-gap dependence on P_V [see Fig. 7(b) and (e)] is almost linear because the increasing number of vacancies blocks the transport due to the decreasing number of available atomic sites and states. Interestingly, wider GNR exhibits a larger gap than the narrower one at very high vacancy density, i.e., P_V of 5% and 10%, but $E_{\rm TG}$ is lower in the 1.84-nm-wide GNR for more realistic P_V. For $P_V = 3\%$, the half gap reaches 0.602 and 0.451 eV for GNR widths of 1.10 and 1.84 nm, respectively. Potential fluctuations [see Fig. 7(c) and (f)] cause a 3%–4% increase of the half gap for the highest amplitude considered. Hence, our results demonstrate that the transport gap of extremely scaled GNRs is immune to potential disorder, as demonstrated experimentally, e.g., by Stampfer *et al.* [28] in larger GNRs ($W \approx 45$ nm and $L \approx 200$ nm). For edge-defected GNRs wider than those shown in Fig. 7, the transmission-based $E_{\rm TG}$ increases by 22%, 20%, and 23% (for $P_{\rm ED}$ of 50%, compared to ideal GNRs) for nanoribbons that are 2.58, 3.32, and 4.06 nm wide, respectively. Hence, in GNRs with edge defects, we observe a generally decreasing $E_{\rm TG}$ enhancement when the GNR width increases, which demonstrates a higher immunity to edge disorder in wider nanoribbons. As for the vacancies and potential fluctuations, wider GNRs exhibit qualitatively identical behavior as the two narrowest GNRs, i.e., an almost linear dependence of $E_{\rm TG}$ on P_V and a negligible influence of potential fluctuations.

The variation of $E_{\rm TG}$ values from device to device is very important from the reliability point of view. We report the standard deviation (σ) of $E_{\rm TG}$ given as a percentage of the average $E_{\rm TG}$ obtained for a given width and disorder strength. For $W = 1.10$ nm, we obtain σ of up to 31.6%, 20.5%, and 6.9% in the case of edge defects, vacancies, and fluctuations, respectively. Similarly, maximum deviations for the 1.84-nm-wide nanoribbon are 27.3%, 23.6%, and 7.5%, which are quite close to the values obtained for $W = 1.10$ nm. We have also analyzed edge-defected GNRs with the widths of up to ~4 nm and found that the maximum standard deviations are 28.2%, 33.6%, and 34.7% for W of 2.58, 3.32, and 4.06 nm, respectively. Therefore, we do not observe a clear trend in $E_{\rm TG}$ deviation versus GNR width for edge-defected GNRs, i.e., σ is close to 30% for all devices considered in this work. From the results presented earlier, the rather high variation of $E_{\rm TG}$ from device to device could be the most important limiter for the possible CMOS application of extremely scaled GNRs.

The behavior of DOS and transport gap reported so far in this paper is vital for carrier mobility modeling within the semiclassical approach based on the Kubo–Greenwood formalism and the calculation of scattering rates. Namely, as shown in [30], [34], and [35], the scattering spectra of relevant scattering mechanisms in GNRs depend directly on DOS that is heavily influenced by disorder. Hence, the deformation of the Van Hove singularities, the nonzero DOS in the gap, and the effects of disorder on the transport gap and its variation should be accounted for when calculating carrier mobility in GNRs.

In order to study the influence of disorder on the ON-state and OFF-state ($G_{\rm OFF}$) conductances and ON–OFF conductance

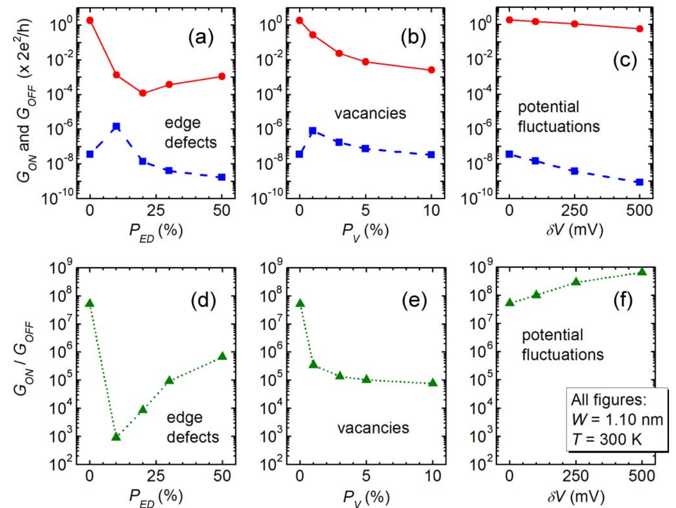

Fig. 8. For the 1.10-nm-wide GNR, the dependence of (full line) $G_{\rm ON}$ and (dashed line) $G_{\rm OFF}$ on disorder strength is shown in (a)–(c), while the dependence of (dotted line) $G_{\rm ON}/G_{\rm OFF}$ ratio on $P_{\rm ED}$, P_V, and δV is presented in (d)–(f). Conductances are calculated for 300 K.

ratio, we calculate the conductances at 300 K using

$$G = \frac{2e^2}{h} \int_0^\infty dE\, T(E) \left[-\frac{\partial f(E)}{\partial E} \right] \tag{4}$$

where $T(E)$ is the averaged transmission function for a given device and disorder strength, $f(E)$ is the Fermi–Dirac distribution function, and h is the Planck's constant. We define $G_{\rm ON}$ at $E_F = 0.7$ eV because 0.7 V is the projected $V_{\rm DD}$ for the 12-nm CMOS node [2], while $G_{\rm OFF}$ is calculated for $E_F = 0$ eV. Fig. 8 presents the conductance and ratio results for $W = 1.10$ nm. Generally, both the ON- and OFF-state conductances decrease as disorder strength increases due to suppressed transmission, while $G_{\rm ON}$ surprisingly exhibits a minimum for $P_{\rm ED} = 20\%$. We attribute this behavior to the occurrence of transmission peaks inside the transport gap when $P_{\rm ED}$ increases [see Fig. 2(b)]. For $P_{\rm ED} > 20\%$, $G_{\rm ON}$ increases because the weight function $\partial f/\partial E$ in (4) encompasses the local transmission peaks in the calculation of the ON-state conductance [cf. transmission curves around $E = 0.7$ eV in Fig. 2(b)]. Interestingly, $G_{\rm OFF}$ is higher in defected GNRs with $P_{\rm ED} = 10\%$ and $P_V = 1\%$ than in the ideal GNR [see Fig. 8(a) and (b)] due to the existence of localized states with relatively high transmission near $E = 0$ eV. For higher disorder strengths, $G_{\rm OFF}$ decreases due to stronger localization effects and the increase of the transport gap. With the increasing disorder strength, the ON–OFF conductance ratio shown in Fig. 8(d)–(f) increases in edge-defected GNRs and GNRs with potential fluctuations due to the stronger decrease of $G_{\rm OFF}$ than of $G_{\rm ON}$, whereas in the case of vacancies, $G_{\rm ON}/G_{\rm OFF}$ decreases with increasing P_V. The maximum ratio for edge-defected GNRs with $W = 1.10$ nm is $6.6 \cdot 10^5$. The results for the 1.84-nm-wide GNR are shown in Fig. 9, where similar trends can be observed as in the case where $W = 1.10$ nm, i.e., $G_{\rm ON}$ and $G_{\rm OFF}$ decrease with increasing disorder strength and $G_{\rm ON}/G_{\rm OFF}$ increases in GNRs with edge defects and potential fluctuations. The major dissimilarity between the two devices

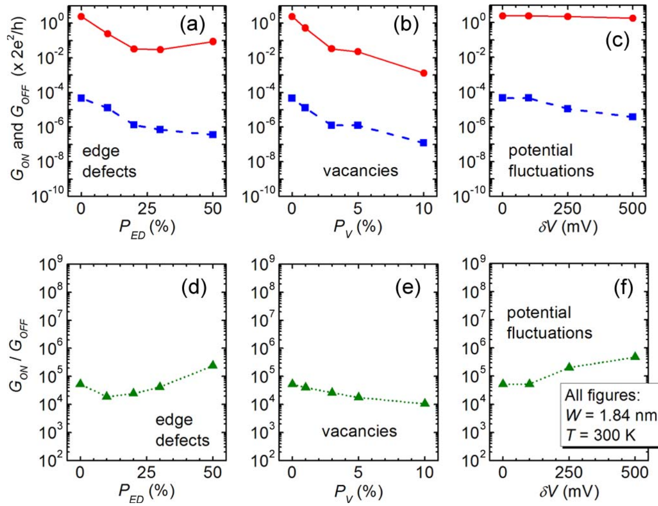

Fig. 9. (Full line) G_{ON} and (dashed line) G_{OFF} versus disorder strength for $W = 1.84$ nm are shown in (a)–(c), whereas the dependence of $G_{\mathrm{ON}}/G_{\mathrm{OFF}}$ ratio on P_{ED}, P_V, and δV is presented in (d)–(f) with a dotted line. Conductances are calculated for 300 K.

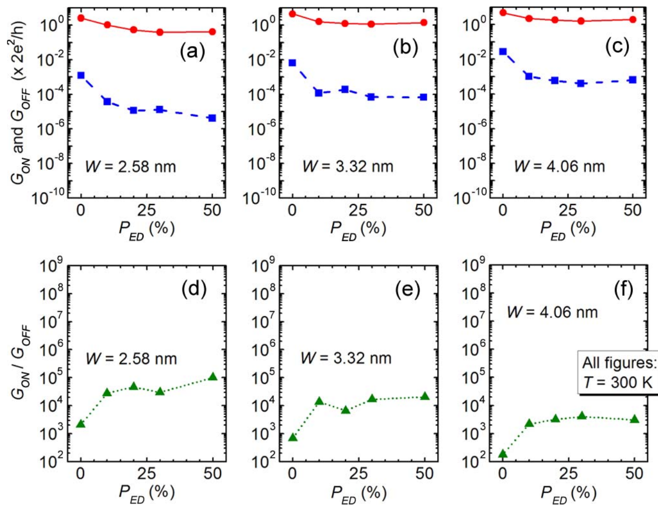

Fig. 10. Influence of different edge-defect densities on (full line) G_{ON} and (dashed line) G_{OFF} is shown in (a)–(c), whereas the behavior of the $G_{\mathrm{ON}}/G_{\mathrm{OFF}}$ ratio is presented in (d)–(f). GNR widths are [(a) and (d)] 2.58 nm, [(b) and (e)] 3.32 nm, and [(c) and (f)] 4.06 nm.

is that the wider GNR exhibits a smaller difference between the ideal GNR and defected GNRs with $P_{\mathrm{ED}} = 10\%$ and $P_V = 1\%$ and a less noticeable G_{ON} minimum for edge-defected GNRs, which indicates weaker effects of local transmission peaks in wider GNRs [36]. The ON–OFF conductance ratio for $W = 1.84$ nm and $P_{\mathrm{ED}} = 50\%$ equals $2.4 \cdot 10^5$, which is comparable to that of the 1.10-nm-wide GNR, and agrees to the order of magnitude with the experimentally obtained ON–OFF ratios for the 1–2-nm-wide GNRs in [9]. This indicates that even the smoothest fabricated extremely narrow GNRs exhibit a high edge-defect density. Here, we quantitatively compare only the $G_{\mathrm{ON}}/G_{\mathrm{OFF}}$ calculated for edge-defected nanoribbons because the GNRs in [9] are fabricated by the unzipping of carbon nanotubes and are expected to have a negligible density of vacancies. As shown in Fig. 10, wider GNRs with edge defects (widths of 2.58, 3.32, and 4.06 nm) exhibit similar conductance and ON–OFF ratio dependence on P_{ED}, compared to each other and to the two narrowest GNRs (see Figs. 8 and 9). We observe that G_{ON} and G_{OFF} generally decrease, while $G_{\mathrm{ON}}/G_{\mathrm{OFF}}$ increases with increasing P_{ED}. As the GNR width increases, the maximum ON–OFF conductance ratio decreases from $9.8 \cdot 10^4$, over $2.0 \cdot 10^4$, down to $3.1 \cdot 10^3$ for W of 2.58, 3.32, and 4.06 nm, respectively. Strikingly, the ratio is two orders of magnitude lower in the widest nanoribbon compared to the 1.10-nm-wide GNR, which agrees with the strong $G_{\mathrm{ON}}/G_{\mathrm{OFF}}$ decrease in wider GNRs reported experimentally in [9].

The variation of the ratio is described by the standard deviation of $\log[G_{\mathrm{ON}}/G_{\mathrm{OFF}}]$, given as a percentage of the average value. For $W = 1.10$ nm, the maximum σ equals 47.9%, 38.7%, and 5.4%, whereas the deviation obtained for the 1.84-nm-wide GNR is 26.2%, 37.5%, and 7.3%, for edge defects, vacancies, and potential fluctuations, respectively. Similarly to the variation of E_{TG}, potential fluctuations exhibit the weakest effect, while lattice defects cause a significant variation of $G_{\mathrm{ON}}/G_{\mathrm{OFF}}$ from device to device. The deviation of $\log[G_{\mathrm{ON}}/G_{\mathrm{OFF}}]$ in wider edge-defected GNRs is 19.5%, 17.7%, and 18.2% for the widths of 2.58, 3.32, and 4.06 nm, respectively. The results indicate that the variation of the ON–OFF conductance ratio in edge-defected GNRs decreases in wider nanoribbons, whereas vacancies and potential fluctuations cause similar deviations irrespective of the nanoribbon width.

IV. Conclusion

We have investigated the effects of different disorders on the transport properties of extremely scaled GNRs (with device size for the 12-nm CMOS node) using atomistic NEGF simulations. The transport gap is extracted directly from the transmission characteristics and using an LDOS-based parameter that can differentiate localized and extended states and hence supply the bandgap within the mobility-edge approach. We report E_{TG} dependence on the density of edge defects and vacancies and on the amplitude of potential fluctuations. For realistic P_{ED}, the gap increase caused by edge defects is 23% to 299%, when scaling the GNR width from 4.06 nm down to 1.10 nm. We find that the mobility-edge approach is unsuitable for the extraction of the transport gap in extremely scaled GNRs due to the discrepancy with E_{TG} values extracted directly from transmission functions. We have also examined the behavior of the ON- and OFF-state conductances and the ON–OFF ratio at 300 K. Generally, G_{ON} and G_{OFF} decrease as disorder strength increases. With the increase of P_{ED}, P_V, and δV, the ON–OFF ratio increases in the case of edge defects and fluctuations, while it decreases in GNRs with vacancies, for all GNRs investigated. The narrowest edge-defected GNRs investigated (1–2 nm wide) with a P_{ED} of 50% exhibit an ON–OFF conductance ratio of $\sim 10^5$, which matches the available experimental data for extremely narrow GNRs and indicates that even the smoothest fabricated GNRs exhibit a high edge-defect density. We have calculated the standard deviation of E_{TG} and of the exponent $\log[G_{\mathrm{ON}}/G_{\mathrm{OFF}}]$, and our results demonstrate a rather high variation from device to device, i.e., σ of up to 35% for E_{TG} and up to 48% for the ON–OFF ratio. The variation of the transport properties caused by defects could be a strong limiter for the nanoelectronics applications of extremely scaled GNRs.

REFERENCES

[1] T. Skotnicki, C. Fenouillet-Beranger, C. Gallon, F. Buf, S. Monfray, F. Payet, A. Pouydebasque, M. Szczap, A. Farcy, F. Arnaud, S. Clerc, M. Sellier, A. Cathignol, J.-P. Schoellkopf, E. Perea, R. Ferrant, and H. Mingam, "Innovative materials, devices, and CMOS technologies for low-power mobile multimedia," *IEEE Trans. Electron Devices*, vol. 55, no. 1, pp. 96–130, Jan. 2008.

[2] International Technology Roadmap for Semiconductors (ITRS), 2011 Edition. [Online]. Available: http://www.itrs.net

[3] K. S. Novoselov, A. K. Geim, S. V. Morozov, D. Jiang, Y. Zhang, S. V. Dubonos, I. V. Grigorieva, and A. A. Firsov, "Electric field effect in atomically thin carbon films," *Science*, vol. 306, no. 5696, pp. 666–669, Oct. 2004.

[4] G. Liang, N. Neophytou, D. E. Nikonov, and M. S. Lundstrom, "Performance projections for ballistic graphene nanoribbon field-effect transistors," *IEEE Trans. Electron Devices*, vol. 54, no. 4, pp. 677–682, Apr. 2007.

[5] Y. Ouyang, Y. Yoon, and J. Guo, "Scaling behaviors of graphene nanoribbon FETs: A three-dimensional quantum simulation study," *IEEE Trans. Electron Devices*, vol. 54, no. 9, pp. 2223–2231, Sep. 2007.

[6] W. S. Hwang, K. Tahy, X. Li, H. Xing, A. C. Seabaugh, C. Y. Sung, and D. Jena, "Transport properties of graphene nanoribbon transistors on chemical-vapor-deposition grown wafer-scale graphene," *Appl. Phys. Lett.*, vol. 100, no. 20, pp. 203 107-1–203 107-3, May 2012.

[7] K. Wakabayashi, M. Fujita, H. Ajiki, and M. Sigrist, "Electronic and magnetic properties of nanographite ribbons," *Phys. Rev. B*, vol. 59, no. 12, pp. 8271–8282, Mar. 1999.

[8] M. Y. Han, B. Özyilmaz, Y. Zhang, and P. Kim, "Energy band-gap engineering of graphene nanoribbons," *Phys. Rev. Lett.*, vol. 98, no. 20, p. 206 805, May 2007.

[9] X. Li, X. Wang, L. Zhang, S. Lee, and H. Dai, "Chemically derived, ultrasmooth graphene nanoribbon semiconductors," *Science*, vol. 319, no. 5867, pp. 1229–1232, Jan. 2008.

[10] D. Querlioz, Y. Apertet, A. Valentin, K. Huet, A. Bournel, S. Galdin-Retailleau, and P. Dollfus, "Suppression of the orientation effects on bandgap in graphene nanoribbons in the presence of edge disorder," *Appl. Phys. Lett.*, vol. 92, no. 4, pp. 042108-1–042108-3, Jan. 2008.

[11] E. H. Hwang, S. Adam, and S. Das Sarma, "Carrier transport in two-dimensional graphene layers," *Phys. Rev. Lett.*, vol. 98, no. 18, p. 186 806, May 2007.

[12] V. M. Pereira, J. M. B. Lopes dos Santos, and A. H. Castro Neto, "Modeling disorder in graphene," *Phys. Rev. B*, vol. 77, no. 11, p. 115 109, Mar. 2008.

[13] Y. Sui, T. Low, M. Lundstrom, and J. Appenzeller, "Signatures of disorder in the minimum conductivity of graphene," *Nano Lett.*, vol. 11, no. 3, pp. 1319–1322, Mar. 2011.

[14] D. Gunlycke, D. A. Areshkin, and C. T. White, "Semiconducting graphene nanostrips with edge disorder," *Appl. Phys. Lett.*, vol. 90, no. 14, pp. 142104-1–142104-3, Apr. 2007.

[15] Y. Yoon and J. Guo, "Effect of edge roughness in graphene nanoribbon transistors," *Appl. Phys. Lett.*, vol. 91, no. 7, pp. 073103-1–073103-3, Aug. 2007.

[16] D. Basu, M. J. Gilbert, L. F. Register, S. K. Banerjee, and A. H. MacDonald, "Effect of edge roughness on electronic transport in graphene nanoribbon channel metal-oxide-semiconductor field-effect transistors," *Appl. Phys. Lett.*, vol. 92, no. 4, pp. 042114-1–042114-3, Jan. 2008.

[17] E. R. Mucciolo, A. H. Castro Neto, and C. H. Lewenkopf, "Conductance quantization and transport gaps in disordered graphene nanoribbons," *Phys. Rev. B*, vol. 79, no. 7, p. 075407, Feb. 2009.

[18] T. C. Li and S.-P. Lu, "Quantum conductance of graphene nanoribbons with edge defects," *Phys. Rev. B*, vol. 77, no. 8, p. 085408, Feb. 2008.

[19] J. J. Palacios, J. Fernández-Rossier, and L. Brey, "Vacancy-induced magnetism in graphene and graphene ribbons," *Phys. Rev. B*, vol. 77, no. 19, p. 195 428, May 2008.

[20] Y. Hancock, A. Uppstu, K. Saloriutta, A. Harju, and M. J. Puska, "Generalized tight-binding transport model for graphene nanoribbon-based systems," *Phys. Rev. B*, vol. 81, no. 24, p. 245 402, Jun. 2010.

[21] Y.-W. Son, M. L. Cohen, and S. G. Louie, "Energy gaps in graphene nanoribbons," *Phys. Rev. Lett.*, vol. 97, no. 21, p. 216 803, Nov. 2006.

[22] R. Sako, H. Hosokawa, and H. Tsuchiya, "Computational study of edge configuration and quantum confinement effects on graphene nanoribbon transport," *IEEE Electron Device Lett.*, vol. 32, no. 1, pp. 6–8, Jan. 2011.

[23] S. Datta, *Quantum Transport: Atom to Transistor*, 2nd ed. Cambridge, U.K.: Cambridge Univ. Press, 2005.

[24] R. Golizadeh-Mojarad and S. Datta, "Nonequilibrium Green's function based models for dephasing in quantum transport," *Phys. Rev. B*, vol. 75, no. 8, p. 081301, Feb. 2007.

[25] A. Yazdanpanah, M. Pourfath, M. Fathipour, H. Kosina, and S. Selberherr, "A numerical study of line-edge roughness scattering in graphene nanoribbons," *IEEE Trans. Electron Devices*, vol. 59, no. 2, pp. 433–440, Feb. 2012.

[26] C. H. Lewenkopf, E. R. Mucciolo, and A. H. Castro Neto, "Numerical studies of conductivity and Fano factor in disordered graphene," *Phys. Rev. B*, vol. 77, no. 8, p. 081410, Feb. 2008.

[27] J. Martin, N. Akerman, G. Ulbricht, T. Lohmann, J. H. Smet, K. von Klitzing, and A. Yacoby, "Observation of electron-hole puddles in graphene using a scanning single-electron transistor," *Nat. Phys.*, vol. 4, no. 2, pp. 144–148, Feb. 2008.

[28] C. Stampfer, J. Güttinger, S. Hellmüller, F. Molitor, K. Ensslin, and T. Ihn, "Energy gaps in etched graphene nanoribbons," *Phys. Rev. Lett.*, vol. 102, no. 5, p. 056403, Feb. 2009.

[29] H. Xu, T. Heinzel, and I. V. Zozoulenko, "Geometric magneto-conductance dips by edge roughness in graphene nanoribbons," *Europhys. Lett.*, vol. 97, no. 2, p. 28 008, Jan. 2012.

[30] M. Bresciani, P. Palestri, D. Esseni, and L. Selmi, "Simple and efficient modeling of the E-k relationship and low-field mobility in graphene nano-ribbons," *Solid State Electron.*, vol. 54, no. 9, pp. 1015–1021, Sep. 2010.

[31] M. Y. Han, J. C. Brant, and P. Kim, "Electron transport in disordered graphene nanoribbons," *Phys. Rev. Lett.*, vol. 104, no. 5, p. 056801, Feb. 2010.

[32] A. Miller and E. Abrahams, "Impurity conduction at low concentrations," *Phys. Rev.*, vol. 120, no. 3, pp. 745–755, Nov. 1960.

[33] N. F. Mott, "Conduction in glasses containing transition metal ions," *J. Non-Cryst. Solids*, vol. 1, no. 1, pp. 1–17, Dec. 1968.

[34] T. Fang, A. Konar, H. Xing, and D. Jena, "Mobility in semiconducting graphene nanoribbons: Phonon, impurity, and edge roughness scattering," *Phys. Rev. B*, vol. 78, no. 20, p. 205 403, Nov. 2008.

[35] A. Betti, G. Fiori, and G. Iannaccone, "Atomistic investigation of low-field mobility in graphene nanoribbons," *IEEE Trans. Electron Devices*, vol. 58, no. 9, pp. 2824–2830, Sep. 2011.

[36] M. Poljak, E. B. Song, M. Wang, T. Suligoj, and K. L. Wang, "Effects of disorder on transport properties of graphene nanoribbons," in *Proc. Eur. Solid-State Device Res. Conf.*, Bordeaux, France, Sep. 2012.

Mirko Poljak (S'07) received the Dipl.Ing. degree in electrical engineering from the University of Zagreb, Zagreb, Croatia, in 2007, where he is currently working toward the Ph.D. degree.

He is currently with the University of California at Los Angeles, Los Angeles.

Emil B. Song received the M.S. degree in electrical engineering from the University of California at Los Angeles, Los Angeles, in 2009, where he is currently working toward the Ph.D. degree.

Minsheng Wang received the B.S. and M.S. degrees in electrical engineering from Tsinghua University, Beijing, China, in 2002 and 2005, respectively. He is currently working toward the Ph.D. degree at the University of California at Los Angeles, Los Angeles.

Tomislav Suligoj (M'00) received the Ph.D. degree from the University of Zagreb, Zagreb, Croatia, in 2001.

He is an Associate Professor of microelectronics and semiconductor technology with the University of Zagreb.

Kang L. Wang (F'92) received the Ph.D. degree from Massachusetts Institute of Technology, Cambridge, MA, in 1970.

In 1979, he joined the University of California at Los Angeles, Los Angeles, where he is currently a Professor of Physical Science and Electronics.